SLOVENSKÁ TECHNICKÁ
UNIVERZITA V BRATISLAVE
FAKULTA ELEKTROTECHNIKY
A INFORMATIKY

**Ing. Jaroslav Dzuba**

**Autoreferát dizertačnej práce**

# DESIGN OF ALGAN/GAN MEMS PRESSURE SENSOR FOR HARSH ENVIRONMENT
# NÁVRH ALGAN/GAN MEMS TLAKOVÉHO SENZORA PRE NEHOSTINNÉ PROSTREDIA

**na získanie** vedecko-akademickej hodnosti doktor *philosophiae doctor*

**v doktorandskom študijnom programe:** **Mikroelektronika**
**v študijnom odbore** 5.2.13 Mikroelektronika

**Miesto a dátum:** Bratislava, 9.7.2015

**Dizertačná práca bola vypracovaná** v dennej forme doktorandského štúdia

**Na** Elektrotechnickom ústave Slovenskej akadémie vied
Dúbravská cesta 9, 841 04 Bratislava

**Predkladateľ:** Ing. Jaroslav Dzuba
Elektrotechnický ústav SAV
Dúbravská cesta 9, 841 04 Bratislava

**Školiteľ:** Ing. Gabriel Vanko, PhD.
Elektrotechnický ústav SAV
Dúbravská cesta 9, 841 04 Bratislava

**Oponenti:**

**Autoreferát bol rozoslaný:** .....
**Obhajoba dizertačnej práce sa koná:** ..... o ..... h.

**Na** Elektrotechnickom ústave SAV
Dúbravská cesta 9, 841 02 Bratislava

Prof. Dr. Ing. Miloš Oravec
Dekan FEI STU v Bratislave
Ilkovičova 3, 812 19 Bratislava

# Table of Contents

# 1. Introduction

The motivation for this research lies primarily in the need to design and fabricate the miniaturized pressure sensors able to withstand the harsh conditions. The microscale pressure sensors are type of a micro-electro-mechanical system (MEMS) that operates on the principle of mechanical deformation and stress change of thin diaphragms. The use of Si-based electronics is restricted in harsh environments, i.e. in chemically aggressive environment or when they operate at high temperatures. In this case, the III-nitrides (III-N) group provides advantageous properties what makes these materials to be preferable for using in such conditions. They are very attractive for pressure and stress sensor applications because of their excellent piezoelectric properties. Compared with the other commonly used piezoelectrics, the III-Ns provides important advantages: compatibility with standard high electron mobility transistor (HEMT) technology, high mechanical stability of epitaxial films and possibility to be used at high temperatures because their piezoelectric properties are preserved in a wide temperature range [1–3].

In this thesis, the specific III-N compounds (AlGaN, GaN) are used to create the piezoelectric MEMS pressure sensor. A conductive two dimensional electron gas (2DEG) is created by interconnecting these two materials into the heterostructure. The piezoelectric polarization and conductivity of the 2DEG channel in the nitride layers can be changed by external mechanical forces. Therefore the heterostructure can read the pressure through the HEMT device integrated. Moreover the 2DEG can also be utilized otherwise. Thanks to the piezoelectric properties of III-Ns, a piezoelectric sensitive layer is created by the HEMT device cross-sectional configuration [4, 5]. The 2DEG is then used as the bottom sensing electrode connected with piezoelectric AlGaN barrier layer. The second collecting electrode is created by the gate electrode of the HEMT device. The piezoelectric charge is generated between two sensing electrodes while the AlGaN/GaN diaphragm is mechanically loaded.

Micromachining of the III-N semiconductors is relatively a new technology. High mechanical stability of the AlGaN/GaN heterostructure makes it very difficult to be etched into the design applicable for pressure sensing, i.e. diaphragm. Hence we decided to use well-developed micromachining of silicon (Si) and therefore, the supplied AlGaN/GaN heterostructure was preferentially grown on Si substrate. Then the convenient AlGaN/GaN diaphragms are manufactured by deep reactive ion etching (DRIE) of the Si substrate from bottom side. Finally, the functionality of proposed AlGaN/GaN piezoelectric MEMS pressure sensor working on direct piezoelectric effect is verified by both the measuring and the simulation of piezoelectric response of the MEMS sensor under the dynamic pressure load.

# 2. Goals of dissertation thesis

Within the scope of this thesis, the following goals are stated:

- Verification of the functionality of the proposed AlGaN/GaN MEMS pressure sensor according to the piezoelectric sensing principle.
- Determination of the mechanical and piezoelectric behavior of the diaphragm-based pressure sensor using the experimental measurement and the FEM modeling.
- Investigation of the residual stress in the thin AlGaN/GaN layers of proposed MEMS pressure sensor using various experimental methods.
- Creation of the FEM model of the MEMS pressure sensor which includes the initially stressed diaphragm and reflects behavior of the real manufactured device.
- Experimental investigation of the piezoelectric response of the MEMS pressure sensor and its comparison with the simulated piezoelectric charge.
- Optimization of the FEM model in order to maximize the piezoelectric charge readout with regard to the distribution of mechanical stress in the loaded diaphragm.

# 3. Current state-of-the-art in AlGaN/GaN-based MEMS pressure sensors

Recently, the Si-based MEMS were mainly used in pressure sensing because of low cost and ease of circuit integration. In the present, we can see the appearance of alternative material systems. Material group III-Nitrides (III-Ns) is very attractive for pressure and strain sensor applications due to their excellent piezoelectric properties [3]. Commonly, the AlGaN/GaN-based devices exploit a fact that the piezoelectric polarization in the nitride layer can be changed by the external forces. This change causes the corresponding change in the density of the two dimensional electron gas (2DEG) confined at the AlGaN/GaN heterointerface. As a result, the change in the HEMT conductivity can be obtained which is directly related to the external strain. Therefore, HEMTs, Schottky diodes and resistors based on the AlGaN/GaN heterostructures could be very useful as sensing devices, especially for application in harsh environment, e.g. in the combustion engine, exhaust, etc. [2].

To investigate the piezoelectric response of III-N devices, various approaches were reported, e.g. bulk device approach, devices integrated on a bulk substrate cantilevers, or devices integrated on membrane structures. In the first approach, the device does not require the realization of suspended microstructure. The function is based on the action of hydrostatic pressure which alters Ni/Au/GaN and Ni/AlGaN Schottky barrier height [6, 7], respectively, the internal fields in GaN/AlGaN/GaN heterostructures [8] and the polarization in AlGaN/GaN heterostructure [9]. In the second approach, the AlGaN/GaN HEMT process technology is performed on a bulk sapphire or SiC substrate. The substrate with the integrated HEMT as a strain sensor is then cut out into a bulk cantilever structure which is then exposed to bending [4, 5, 10–16]. The resulted channel resistivity is measured in dependence on applied strain. In third approach, the potential of III-Ns for pressure sensors based on membrane or diaphragm structures integrated with HEMT sensing device is much less evaluated in compare with SiC or sapphire bulk devices. The difficulty to fabricated suspended AlGaN/GaN heterostructure arises from the high mechanical stability of III-N material group, which complicates the necessary undercutting techniques. A promising approach is the deposition of AlGaN/GaN heterostructure on Si. Despite the high prospects of the 2DEG for mechanical sensors with internal amplification, only a few reports on membrane test structures are available [3, 17]. The pressure induced changes in the conductivity of AlGaN/GaN HEMT membranes were observed also in [18] where the drain-source current-voltage characteristics of the HEMT were evaluated. The pressure sensor based on the GaN HEMT was proposed e.g. in [19]. Change in the piezo-induced 2DEG density at the AlGaN/GaN interface affected the capacitance of the channel of AlGaN/GaN HEMT diaphragm. The carrier density was therefore directly correlated with the calculated tensile strain in the membrane and hence with the differential pressure acting on the membrane.

Although the AlGaN/GaN diaphragms were successfully manufactured, a fundamental piezoelectric readout of mechanical sensors has not been reported for III-N group. Mostly, the AlGaN/GaN heterostructures are used in active sensing using of HEMT. The sensors based on the piezoelectric sensing have been reported only for GaN-based Schottky diodes [20]. The fundamental principle of piezoelectric sensing was firstly demonstrated by Vanko et al. [4, 5, 5, 14, 15, 21] on bulk SiC cantilever-based structure. A thin piezoelectric element was created by the HEMT device cross-sectional construction (*FIG. 1*). The 2DEG was used as the bottom conductive electrode of the piezoelectric AlGaN barrier layer which generates a piezoelectric charge on the top collecting gate electrode of the HEMT device, while the external mechanical forces were acting on the entire structure. In this thesis, the fundamental piezoelectric readout of the piezoelectric element created from AlGaN/GaN diaphragm is investigated for the first time.

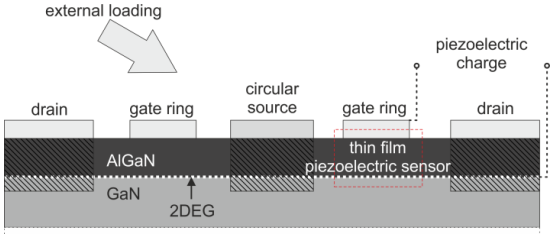


***FIG. 1*** *The piezoelectric charge is generated in AlGaN layer while the device is loaded.*

# 4. Results

## 4.1. FEM model of AlGaN/GaN MEMS pressure sensor

Although the cantilever-based structure demonstrated the functionality of the MEMS sensor to sense the external dynamic stress [4, 5], it was considered to be inappropriate for pressure sensing. The circular symmetry of the 2DEG was fully considered compatible with the circular diaphragm structure preferentially used for MEMS pressure sensors design. Therefore the piezoelectric element created by C-HEMT electrodes was implemented into the diaphragm structure at first (*FIG. 2*). The identical 28 nm/1.9 μm $Al_{0.2}Ga_{0.8}N$/GaN heterostructures as used in cantilever topology [4, 5] were applied in designing the new diaphragm-based sensing structures.

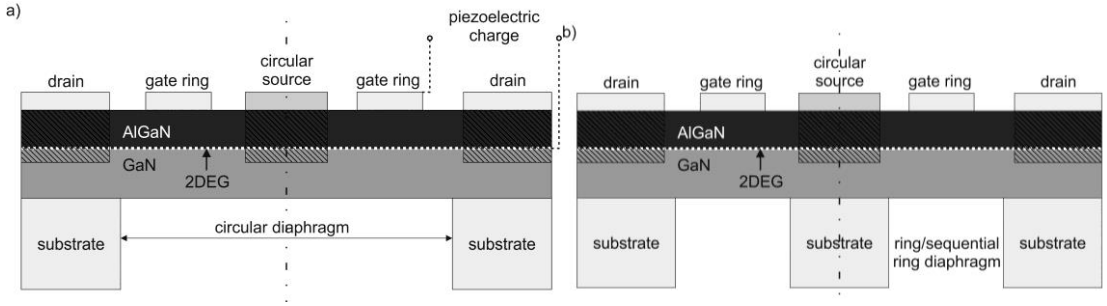


***FIG. 2*** *C-HEMT electrodes implemented into circular (a) and ring/sequential diaphragm (b).*

The SiC substrate material was replaced by the 330 μm thick Si which was locally selective etched to create the suspended diaphragm of circular, ring and sequential ring shape (*FIG. 3*). The diaphragms with outer diameters approximately 480 μm were designed and successfully manufactured in the first step. In some cases, remaining part of the substrate formed the ring or sequential ring diaphragms with diameter of central pillar approximately 120 μm. Next goal was to determine the mechanical and piezoelectric behavior of diaphragm-based pressure sensors. Then, the results can be used in following optimizing process. Two steps were required to achieve this goal: residual stress in the diaphragm needed to be determined and the piezoelectric response should be experimentally investigated and compared with the FEM analysis results.

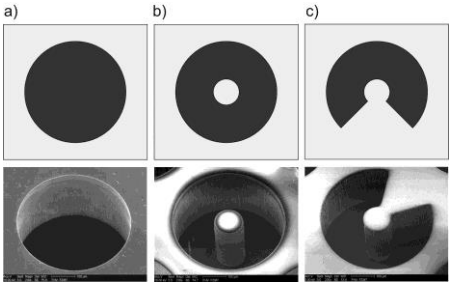


***FIG. 3*** *Sketches of various diaphragm designs and corresponding SEM pictures of manufactured diaphragms: the circular (a), the ring (b) and the sequential ring diaphragm (c).*

Firstly, the residual stress was mapped on the top surface of 1.9 μm thick GaN diaphragms on path starting at the outer radius and ending on the inner radius of the diaphragm (*FIG. 4*). The tensile stress approximately 300 MPa was experimentally determined using the micro-Raman technique and subsequently considered as the initial value of residual stress in the following FEM simulations. The simulated deflection of the sequential ring diaphragm with 240 μm radius was quite low even if the loading pressure was quite high, i.e. static pressure of 10 kPa caused the deflection as small as 0.04 μm. Consequently, the piezoresponse would be very low and insufficient for evaluation by the charge amplifier. Hence the FEM models were modified in the way that the outer radius of diaphragms was increased. We assumed increased deflection of enlarged diaphragms what could lead to the increased sensitivity of the pressure sensor.

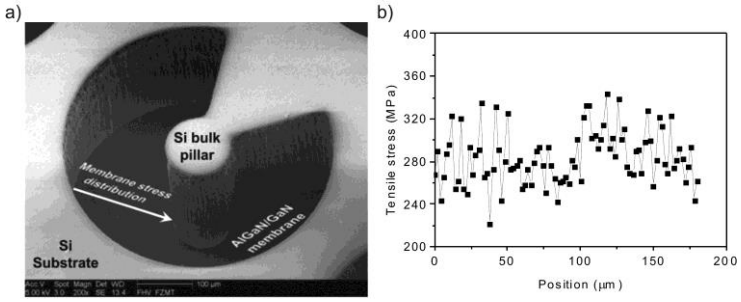


***FIG. 4*** *SEM image of the sequential ring diaphragm structure obtained by DRIE of the 330 μm thick Si substrate with marked direction of stress investigation (a) and distribution of the diaphragm residual stress measured by micro-Raman scattering technique (b).*

So the outer radii of both (circular and ring) diaphragm models were set to 1000 μm. The real structures with these dimensions were planned to be manufactured regarding the results of FEM analyses. The FEM models were created in ANSYS software. The diaphragm of circular/ring was firstly stretched to achieve the desired initial stress and subsequently loaded by the pressure. The goal of this investigation was to determine the optimal position or size of the sensing electrodes and to create a "charge map" which discovers the most appropriate locations for electrodes to maximize the effectiveness of generating the piezoelectric charge. The optimization of the sensing electrodes was based on shifting the electrode with constant width on the surface of diaphragm (*FIG. 5*).

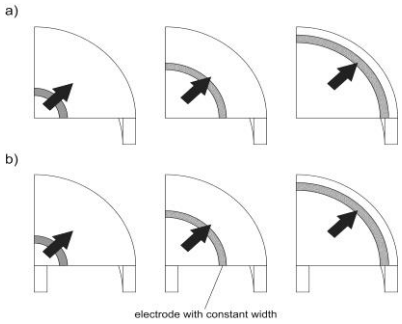


***FIG. 5*** *Optimization of electrode position in the FEM model on the circular diaphragm (a) and ring diaphragm (b) of the AlGaN/GaN MEMS pressure sensor.*

The diaphragm of MEMS pressure sensor is considered with finite thickness so it is not an "ideal membrane". Therefore the behavior of a plate is also incorporated into the general behavior. If the diaphragm is loaded by the pressure, the different stresses are induced on opposite surfaces and the stress varies in radial direction (*FIG. 6*).

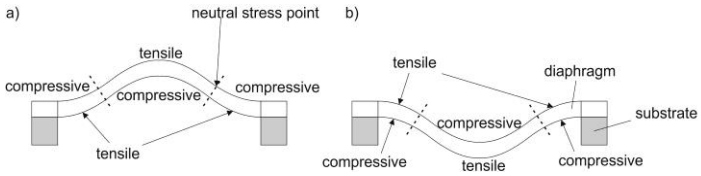


***FIG. 6*** *The mechanical stress changes at surfaces of a diaphragm with fixed edges while bending by pressure. The neutral stress point appears where the surface stress goes to zero.*

A "neutral stress point" occurs at the certain position on the diaphragm. It is a place where the stress changes its character from tensile to compressive or vice versa. From the results of FEM analysis, the various distribution of induced piezoelectric charge can be seen for both diaphragm topologies (*FIG. 7*). At certain position, approximately 950 μm from the center of circular diaphragm (*FIG. 7, a*), the induced charge changes its character from negative to positive. The neutral stress point is located there. Similar effect also occurs in the model of ring diaphragm (*FIG. 7, b*).

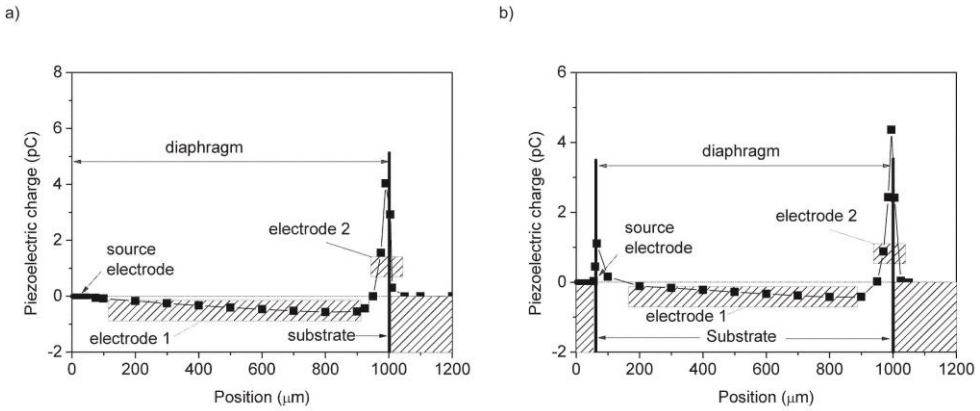


***FIG. 7*** *The FEM calculated distribution of piezoelectric charge on the surface of circular (a) and ring diaphragm (b). Proposed optimal locations of sensing electrodes are marked.*

Following the results of performed simulations, the new electrode layout was designed for the pressure sensors. Subsequently the additional FEM models of the circular diaphragms with varied diameters were simulated (models of diaphragms with 750 and 1500 μm diameter, thickness 1.9 μm). The results showed that the position of the neutral stress point primarily depends of the radius of diaphragm and is located approximately in 95 % of its radius (0.95**R*). For instance, the neutral stress point is situated at position 712 μm for diaphragm with radius 750 μm. If we consider generally the better sensitivity of the circular diaphragms, only the circular design is included in new design proposals of the pressure sensors. The "MESA" design based on additional mesa isolation step and the "$Si_xN_y$" design based on passivation layer were defined (*FIG. 8*).

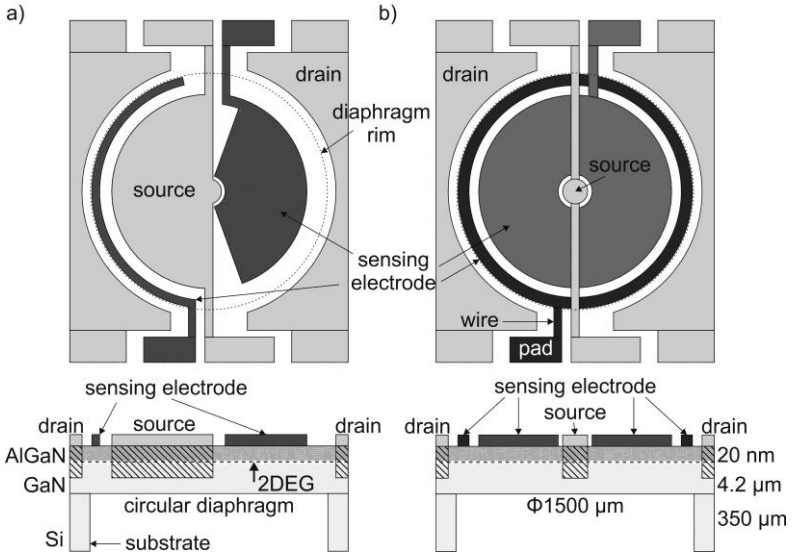


***FIG. 8*** *New design of AlGaN/GaN MEMS pressure sensor developed in consideration of the FEM analyses results: sequential ring or "C shape" electrodes (a) and ring electrodes (b). A simplified schematic cross-section of both designs is outlined below.*

Mesa etching enabled the electrodes to connect separately through the metallic leads to the expanded contacting pads in the MESA design. Consequently, the ring electrodes divided into sequential ring shapes were determined (*FIG. 8, a*). The areas of electrodes are smaller compared to those of ring electrodes of $Si_xN_y$ design (*FIG. 8, b*). In SiN design, the metallic leads that connect the sensing electrodes with the expanded contact pads are placed on silicon nitride layer. Conductive connection with the sensing electrodes is performed through the windows etched in thin $Si_xN_y$ layer. In both new design concepts with 1500 μm diameter, the first sensing electrode was designed with inner and outer radii of 80 and 710 μm, respectively. The second sensing electrode located near the rim of the diaphragm was designed with varied inner and outer radius. Several widths of these electrodes were proposed to obtain varied sensitivity. Three widths of the outer electrode were proposed: 20, 40

and 60 µm. Also the position of the outer electrodes varied in range from 720 to 770 µm. In some cases, the outer electrode was located at the rim of the diaphragm or even exceeded the area of the diaphragm so it was placed partially outside the diaphragm. Mechanical and piezoelectric properties of both designs were then experimentally investigated and compared with results of the FEM analyses.

## 4.2. MEMS pressure sensor technology

Structures on which the previous FEM models were based, exhibited high tensile residual stress (300 MPa) what caused rupture of the diaphragms. Low residual stress in diaphragms was considered to be the key parameter to obtain the function and undamaged MEMS pressure sensors. We assumed that diaphragms made from the low prestressed heterostructure can be loaded by higher pressure than previously investigated diaphragms. Moreover, most of the former diaphragms were ruptured even without loading. In case of low prestressed structures, the total stress, i.e. the sum of residual stress and stress caused by load, would be sufficiently distant from maximum strength of GaN, i.e. 400 MPa of tensile stress [22]. Thus $Al_{0.25}Ga_{0.75}N$/GaN heterostructure on 6" Si substrate was supplied by external manufacturer. The manufacturer stated stress-free or low residual stress what needed to be accurately determined. Therefore the stress was investigated in these structures using of two experimental methods and FEM analysis. The original dimensions of previously used heterostructure (28 nm AlGaN/1.9 µm GaN) were modified by manufacturer (*NTT Advanced Technologies, Japan*) to grow the stress free GaN on Si using of MOCVD technique. The 4.2 µm thick low stressed GaN buffer structure is grown on 600 µm Si substrate. Finally, the 20 nm thin AlGaN barrier layer was grown on GaN buffer layer (*FIG. 9*). The substrate was then grinded to approximately 350 µm. Such thinned structure is prepared for further processing, i.e. serves as a base for the metallization process technology.

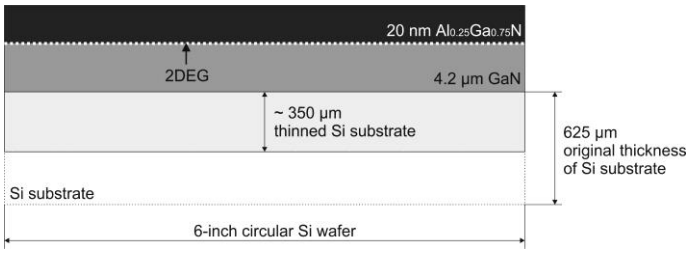


***FIG. 9*** *The AlGaN/GaN heterostructure grown on Si substrate (not in scale). Si substrate is grinded to less difficult micromachining.*

### *4.2.1. MESA design of pressure sensor*

This design does not allow using of full ring area of the sensing electrodes. Instead an adequate sequence of the ring electrode was used. Thus decreased amount of the generated piezoelectric charge was expected. In the MESA design concept, the simple C-HEMT process technology based on mesa etching technique was performed. In the first step, it involves selective etching of the AlGaN layer by reactive ion etching (RIE) in $CCl_4$ plasma. The AlGaN layer is etched out in the areas where the metallic leads will connect the sensing electrodes with the expanded contact pads (*FIG. 10, a*). Therefore this type of sensor is referred as the "sequential ring MESA design" in thesis. In next step, the circular source/drain ohmic contacts of the C-HEMT devices are formed by a sequential electron beam evaporation of Nb/Ti/Al/Ni/Au metallic system with thickness 20/20/120/40/70 nm of material used, followed by the alloying process at 850 °C for 35 s [5]. Then, Ir (15 nm) electron beam evaporation and lift-off technique were carried out subsequently to form the Schottky ring gate contacts of variable area.

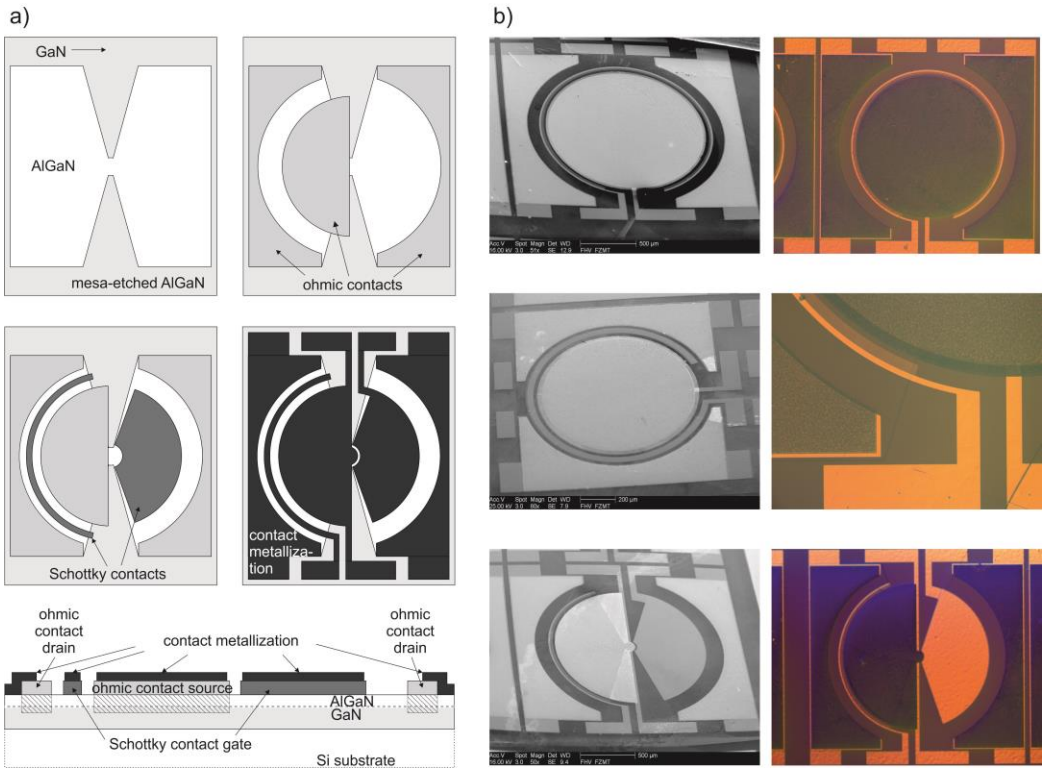


***FIG. 10*** *Manufacturing technology of MESA type of MEMS pressure sensor (a): mesa etching of AlGaN layer, patterning of the ohmic, Schottky sensing and top bonding contact metallization and the cross-section of the final C-HEMT. SEM and optical images of single and double electrode MESA with various electrode widths (b).*

In the last step, Ti/Au (30/120 nm) contact metallization (metallic lead connecting the electrodes and pads) was deposited and formed by lift-off technique on top of the ohmic contacts, respectively. *FIG. 10, b* depicts the scanning electron microscope (SEM) photos of the fabricated MEMS pressure sensors. Various layouts of the MESA sensor were proposed.

### *4.2.2. $Si_xN_y$ design of pressure sensor*

The $Si_xN_y$ design was proposed in order to achieve the maximal charge amount due to using the full area of ring sensing electrode. In this layout, the similar C-HEMT process technology was performed as that in MESA design. However, the process technology omits the mesa etching of AlGaN (*FIG. 11, a*). The metallic leads that connect source, drain and Schottky ring gate electrodes of the C-HEMT with the expanded contact pads are mutually isolated using the insulating $Si_xN_y$ layer. Similarly as in the MESA design, the circular source/drain ohmic contacts were formed by sequential electron beam evaporation using Nb/Ti/Al/Ni/Au metallic system with thickness 20/20/120/40/70 nm of material used and it was followed by alloying at 850 °C for 35 s [5]. Then Ni/Au (40/120 nm) electron beam evaporation and lift off technique were carried out to form the Schottky ring gate contacts of variable area. The isolation and $Si_xN_y$ passivation layer were subsequently deposited on the ohmic and Schottky gate contacts by CVD technique. Then opened windows were created in 100 nm thin $Si_xN_y$ by a selective etching technique in order to connect the sensing electrodes (ohmic and Schottky gate contacts) with the contacting pads through the metallic leads patterned in the last process step. In the last step, Ti/Au (30/120 nm) contact metallization was deposited on top of the isolation layer. The resulted design of the C-HEMT device integrated in the AlGaN/GaN heterostructure can be used to sense pressure when modified by etching the diaphragm.

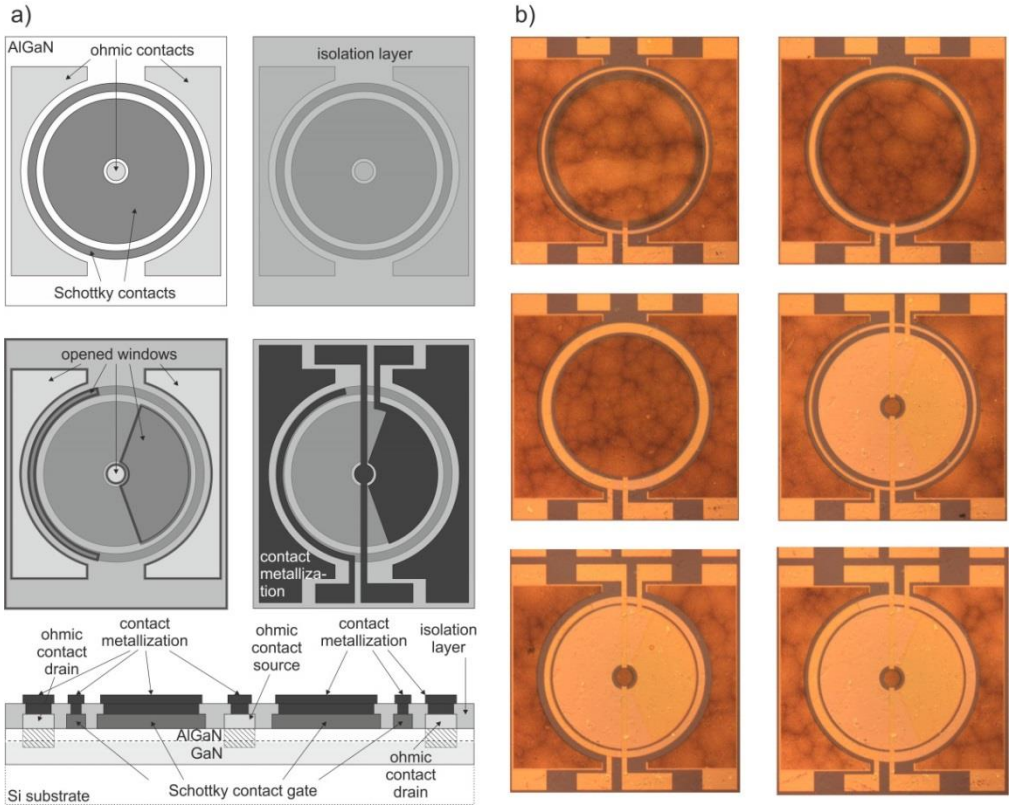


***FIG. 11*** *Manufacturing technology of the $Si_xN_y$ design of the MEMS pressure sensor (a): deposition of ohmic and Schottky gate contacts, deposition of $Si_xN_y$ isolation/passivation layer, etching of the windows into the isolation layer, deposition of contact metallization on top of the isolation layer and cross section of the final C-HEMT. Optical microscope images of the $Si_xN_y$ design (b): single electrode designs in which the narrow gate sensing electrode is located near the rim of diaphragm and the $Si_xN_y$ design with two sensing electrodes.*

The SEM images of various layouts of $Si_xN_y$ MEMS pressure sensors are depicted in *FIG. 11, b*. In alternative design with only one sensing electrode, the source contact with large area is located in the center. The varied width of the outer sensing electrodes can be seen when comparing various modifications of the $Si_xN_y$ pressure sensor.

### *4.2.3. Diaphragm fabrication*

The circular diaphragms of the MEMS pressure sensors were micromachined by the deep reactive ion etching (DRIE) of the thick bearing Si substrate [21]. DRIE has been performed in a time multiplexed inductively coupled plasma (ICP) reactor with $SF_6$ for etching and $C_4F_8$ for sidewall passivation gas mixture.

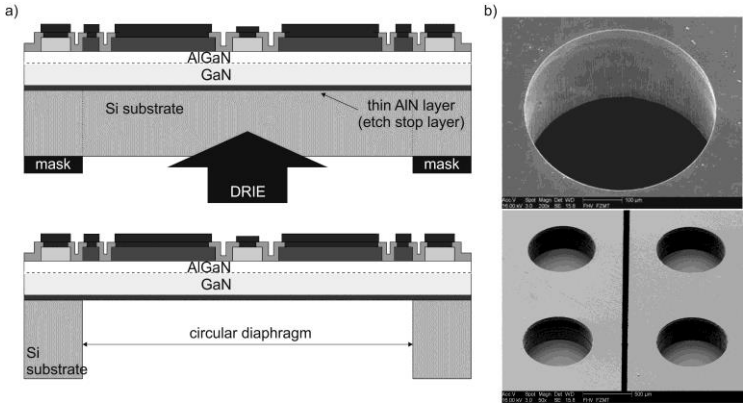


***FIG. 12*** *Deep reactive ion etching (DRIE) of Si substrate performed to create the circular diaphragms consisting the AlGaN/GaN heterostructures (a) and SEM images of the etched circular diaphragms with various diameters (b).*

The AlN interfacial layer (*FIG. 12, a*) served as the etch stop layer of the trench free silicon etching. Low frequency pulsing bias power was used to minimize destructive etching effects at the diaphragm base. Finally, the circular holes with diameters 750, 1000, and 1500 μm were etched.

## 4.3. MEMS pressure sensor performance analysis

Firstly, the residual stress in previously proposed MEMS pressure sensors was examined using of two independent experimental methods supported by the FEM analysis [23]. The resonant frequency method was used to determine the stress in all proposed diaphragms. The static bulging method was performed to determine the residual stress in the largest MEMS sensor including diaphragm with 1500 μm diameter. Consequently, the dynamic piezoelectric responses of the selected MEMS sensor devices were investigated. Dependence of the piezoelectric charge on the frequency of exciting load was studied. The sensitivity of both types of the AlGaN/GaN piezoelectric MEMS pressure sensors and maximum pressure load are determined.

### *4.3.1. Residual stress investigation*

The residual (built-in) stress in the C-HEMT diaphragm-based pressure sensors consisting of 4.2 μm thin $Al_{0.25}Ga_{0.75}N$/GaN diaphragms with diameters 750, 1000 and 1500 μm was investigated. Thickness of the diaphragms is determined by the thickness of the GaN buffer layer (*FIG. 13, a*). Total thickness of nitride diaphragm was measured on the ruptured diaphragm using the SEM software tool. The residual stress in fabricated diaphragms was investigated using of two different experimental techniques. Firstly, the resonant frequency method using laser Doppler vibrometry (LDV) was applied.

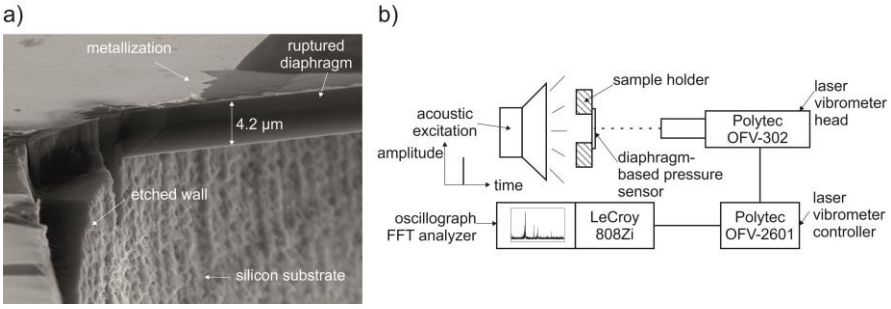


***FIG. 13*** *SEM cross-section view of the AlGaN/GaN diaphragm with specified thickness (a) and the experimental set up scheme for measurement of the diaphragm natural frequencies (b).*

The investigated diaphragms with various diameters were excited by the acoustic pulse (Dirac unit impulse). The excitation was carried out at atmospheric ambient pressure using the experimental scheme depicted in *FIG. 13, b*. The focused spot from the laser vibrometer head *Polytec OFV-302* scanned vibration of the investigated diaphragms. The output signal from vibrometer was processed by the *Polytec OFV-2601* signal controller. Digital oscilloscope *LeCroy 808Zi* with Fourier transform processing was used to evaluate the signal and obtain the frequency spectra of each investigated diaphragm (with 750, 1000 and 1500 μm diameter, MESA type). Visible peaks (*FIG. 14*) at various frequencies are associated with (0,1), (1,1) and (2,1) circular diaphragm modes. Measured spectra for all investigated diaphragms are summarized in *TAB. 1*.

***TAB. 1*** *Comparison of the measured and simulated resonant frequencies of examined diaphragms.*

| | | Mode No. / Res. frequency (kHz) | | |
|---|---|---|---|---|
| Diameter (μm) | Method | 1st mode | 2nd mode | 3rd mode |
| 1500 | Measurement MESA | 52.9 | 90.0 | 142.1 |
| | Measurement $Si_xN_y$ | 50.0 | 87.0 | 143.2 |
| | Simulation (σ=43 MPa) | 52.8 | 90.7 | 131.8 |
| | Deviation (FEM vs. measured MESA) (%) | 0.2 | 0.8 | 7.0 |
| 1000 | Measurement | 76.9 | 146.6 | - |
| | Simulation (σ=21 MPa) | 76.7 | 145.6 | 227.5 |
| | Deviation (%) | 0.3 | 0.7 | - |
| 750 | Measurement | 125.5 | - | - |
| | Simulation (σ=23 MPa) | 125.4 | 244.4 | 387.9 |
| | Deviation (%) | 0.1 | - | - |

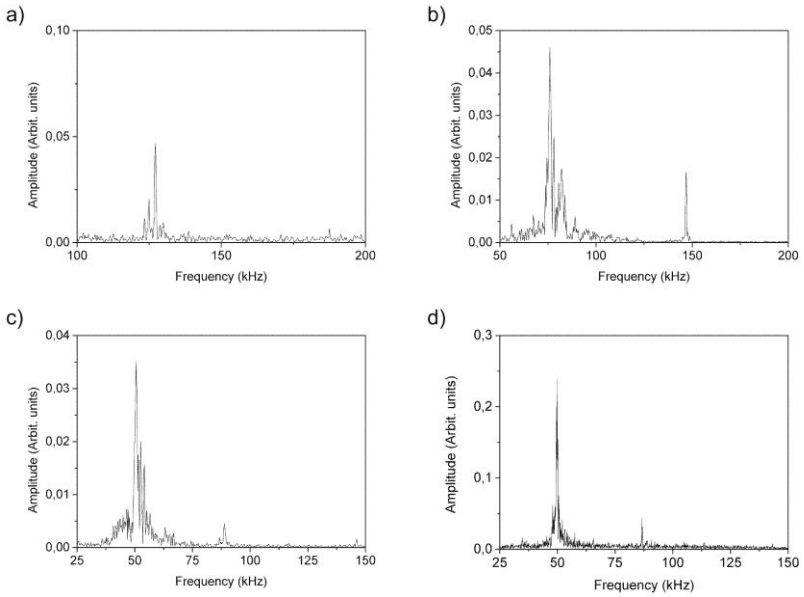


***FIG. 14*** *Characteristic displacement spectra of diaphragm with 750 µm diameter (a), 1000 µm diameter (b), 1500 µm diameter MESA design (c) and 1500 µm diameter $Si_xN_y$ design.*

Almost the same resonant frequency spectrum of the $Si_xN_y$ design with 1500 µm diaphragm was measured as in case of the MESA design with equal diaphragm size. Slightly lower value of the first resonant frequency (MESA vs. $Si_xN_y$, 1500 µm) can be seen from *TAB. 1*. It indicates lower tensile residual stress caused by deposition of the isolation/passivation $Si_xN_y$ layer. The resonant frequency of the other SixNy sensors with 1000 and 750 µm diaphragms were not measured. Considering the small thickness of these diaphragms compared to their diameters, e.g. 1500 µm vs. 4.2 µm, the structures should behave almost as the ideal membranes. However if the ratios of the second and third mode to the first natural mode are plotted, a specific behavior can be seen (*FIG. 15, a*). The measured values lie within the range defined by the known theoretical values of an ideal circular plate and circular membrane. This specific behavior is described by the *k*-parameter which describes the combined behavior of the diaphragm [24, 25].

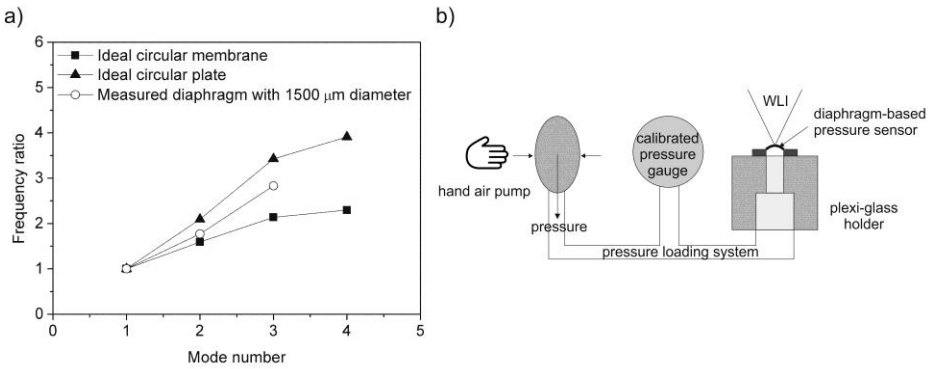


***FIG. 15*** *The ratios of the frequency of different modes to the first fundamental mode of investigated diaphragm with 1500 µm diameter where measured data lie within the range defined by the theoretical values of an ideal circular plate and circular membrane (a) and the customized set-up using WLI to measure the diaphragm bulging during static pressure load applied to bottom side of the investigated MEMS pressure sensor (b).*

Therefore residual stress in investigated diaphragms was calculated using equation which describes the combined behavior of an ideal circular membrane and plate, respectively [26]:

$$f^2 = \left[\frac{2.4048}{2\pi R}\sqrt{\frac{\sigma}{\rho}}\right]^2 + \left[\frac{3.1962^2}{2\pi R}\sqrt{\frac{D_F}{\rho h}}\right]^2, \quad (1)$$

where $D_F$ is the flexural rigidity of the diaphragm with thickness $h$, $R$ is its radius , $f$ is the measured resonant frequency, $\rho$ is mass density of the diaphragms and $\sigma$ is the uniform biaxial tensile stress we calculated. Using of equation (1), the bending stiffness was included in calculation. We assumed the diaphragm consisting of GaN and simplified isotropic material properties for GaN [27]. Consequently, the tensile residual stress was calculated from the measured first natural frequency of each investigated diaphragm: 47 MPa and 41 MPa were calculated for the MESA and $Si_xN_y$ design with the largest diaphragm, respectively. The tensile stresses 22 MPa and 21 MPa were calculated for the MESA diaphragms with diameters 1000 µm and 750 µm. We assumed that the tensile residual stress would have been identical for all the investigated diaphragms and independent on their diameter because the diaphragms were fabricated on the same substrate. The initial (uniform) stress in the heterostructure can be subsequently influenced e.g. by following metallization deposition [28] or deposition of an additional layers such isolation/passivation $Si_xN_y$ layer in $Si_xN_y$ design.

In FEM models we took into account only the final stress state of the diaphragms so we neglected the influence of the additional layers. The FEM simulation was performed to simulate resonant frequencies of the experimentally investigated diaphragms. The anisotropic material properties were input in the FEM model. The goal of modal analysis was to determine the natural mode shapes and frequencies of the modeled diaphragms. In first step of the analysis, the diaphragms were prestressed by the tensile stress calculated from the measured resonant frequencies. Calculated value for each specific diaphragm was set as an initial input value of the built-in stress during the self-consistent solution. Then modal analysis was repeated iteratively by changing the input residual stress to reveal the natural frequencies of all investigated diaphragms until the deviation between the measured and simulated frequency was minimized. The tensile stress of 43 MPa, 21 MPa, and 23 MPa was determined for 1500 µm, 1000 µm, and 750 µm diaphragm, respectively (*TAB. 1*).

To investigate the residual stress in proposed diaphragm-based pressure sensors, the deflection, i.e. bulging method, was additionally performed. Using the customized set-up (*FIG. 15, b*), the investigated diaphragms were loaded by the uniformly distributed static air pressure to their bottom side. This method included the center deflection measurement to obtain the pressure-deflection characteristic which also strongly depends on the residual stress. The non-contact optical white light interferometry (WLI) using *Bruker Contour GT-K1* with 525 nm light wavelength was used to scan the shape of deflected diaphragm while loaded. In this experimental method, only the largest diaphragm with 1500 µm diameter was examined due to the most visibly interference fringes. The uniformly distributed air pressure of 2-14 kPa was applied to the bottom side of the diaphragm and the central deflection was firstly estimated by counting of the interference fringes (*FIG. 16, a*). For accurate determination of the central deflection, the cross sectional deflection profile of optical interferometry was used (*FIG. 16, b*).

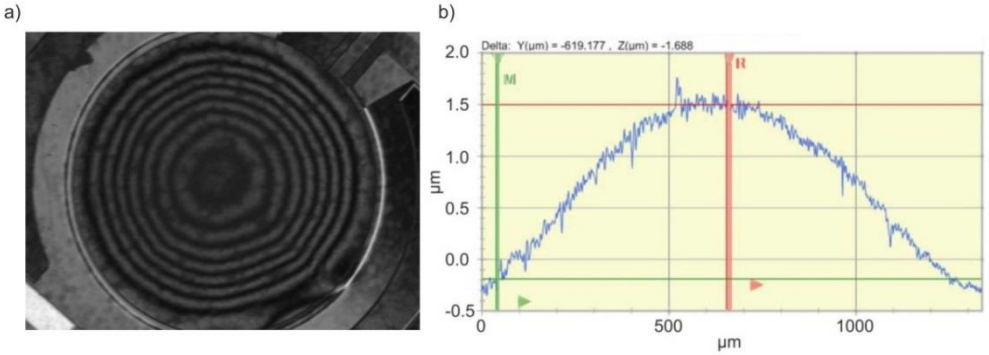


***FIG. 16*** *The interference fringes of the largest deflected diaphragm at 6 kPa pressure (a) and deflected cross section profile of the same diaphragm at 6 kPa applied to bottom side (b).*

The characteristic plate-like behavior of the deflected structure can be seen at the rim of diaphragm where the bending stiffness plays its role. The deflection-pressure characteristic of the loaded diaphragm was experimentally measured (*FIG. 17*). Considering the isotropic material properties and diaphragm consisting only of GaN, the tensile residual stress can be simply determined for each set of applied pressure and the corresponding deflection of diaphragm (deducted from *FIG. 17*) as follows [29]:

$$P = C_0 \frac{E_Y h^3 w}{(1-\vartheta^2)R^4} + C_1 \frac{h\sigma w}{R^2} + C_2 \frac{E_Y h w^3}{(1-\vartheta)R^4}, \qquad (2)$$

where $P$ is the applied pressure, $h$ is thickness and $R$ radius of the diaphragm, $E_Y$ denotes Young's modulus and $\upsilon$ the Poisson's constant, $w$ is the maximal deflection in the center of diaphragm i.e. bulge height and $C_0$, $C_1$, and $C_2$ are dimensionless coefficients that depend on the structure shape [26]. Even if the calculated stress slightly varies for the specific applied pressure, it can be determined as an average value. In this way, the tensile residual stress of approximately 50 MPa was determined for examined diaphragm.

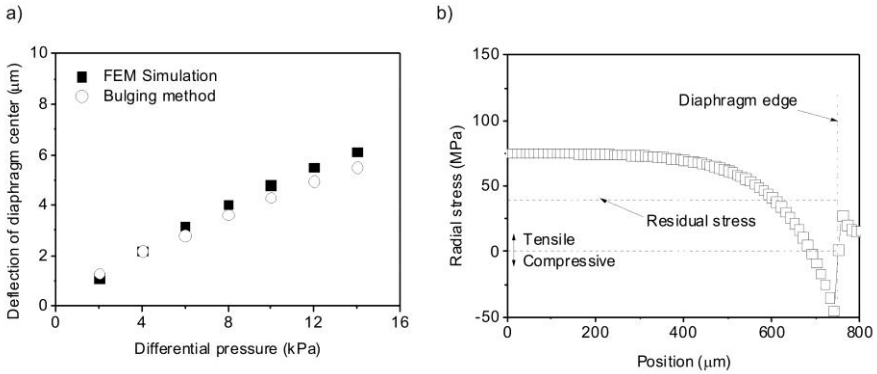


***FIG. 17*** *Measured and simulated deflection response of the largest diaphragm during static pressure load applied to bottom side (a) and in-plane stress on top of the loaded diaphragm with 1500 µm diameter while the static pressure 10 kPa is applied to bottom side of the diaphragm (b).*

The experimental bulging method was confronted with results of the FEM analysis (*FIG. 17, a*) in such way that the tensile stress of 43 MPa determined in the previous FEM experiment (representing the experimental resonant method) was newly prescribed in the FEM model. In this way, the static pressure was applied to the bottom side of prestressed diaphragm. The deflection was expected to be comparable to the thickness of diaphragm so the non-linear static structural analysis was performed. The 43 MPa FEM calculated stress from simulation of experimental resonant method differs from the stress 50 MPa determined by the bulging method using equation 2 by approximately 14 %. Nevertheless, we can say that the stress in the investigated structure was determined quite accurately. Compared to the previously used highly stressed (300 MPa) heterostructures, the new designed heterostructure provides less stressed diaphragms what may result in improved sensitivity.

According to experimentally and FEM obtained results (*FIG. 15*, *FIG. 16*, *FIG. 17, a*), the shape and the resonance of the investigated diaphragm were certainly influenced by both, the tension and the bending stiffness. The character of mechanical radial (in-plane) stress is therefore examined on top of the diaphragm where the sensing electrodes are placed. The result (*FIG. 17, b*) showed a considerable dependence of the in-plane stress on the distance from the diaphragm center which is in position 0 µm. Near the outer edge of the diaphragm (the rim, position 750 µm), the character of stress on top surface changes from the tensile to the compressive/negative values and creates the characteristic edge zone [24]. The neutral stress point should determine the most effective location and/or size of the electrodes, e.g. for piezoelectric charge sensing. The residual stress state of a diaphragm must be taken into account. If the initial residual stress is tensile e.g. 43 MPa as in *FIG. 17, b* then "new neutral stress point" automatically moves to the location where the mechanical stress on top surface of the diaphragm crosses the value 43 MPa. Finally, the extent of edge zone and therefore the in-plane stress in diaphragm caused by pressure load is affected by the residual stress, geometry and material properties. All of these factors are incorporated in *k*-parameter. At high levels of residual stress and/or high pressure load, the mechanical stresses become critical and this zone completely vanishes. Then

the structure behaves like a pure membrane, i.e. ideal membrane. Diaphragms we used in the MEMS pressure sensor cannot achieve such high stress because they would rupture. In the design of pressure sensor, the maximal tensile strength of used material must be considered.

### 4.3.2. Dynamic piezoelectric response

The mechanical and piezoelectric performance of the proposed MEMS pressure sensor was experimentally analyzed during dynamic pressure loading. Several types of the sensors with varied diameters of diaphragms (750-1500 μm) were designed and subsequently fabricated. To present the piezoelectric response, the MEMS sensor with the largest diaphragm with 1500 μm diameter was selected. The sensor can operate on two independent principles: (a) the HEMT principle based on the change of 2DEG channel conductivity with the applied external load [30] and (b) a new principle based on the change of piezoelectric charge induced on the ring gate electrode of C-HEMT with the applied external load [4, 5]. The 2DEG serves as the first sensing electrode of a piezoelectric element. The second collecting electrode is created by the ring gate contact of the C-HEMT. Two different topologies were examined (*FIG. 18*): the MESA design including two sequential ring "C-shape" gate electrodes and the $Si_xN_y$ design including two ring sensing electrodes.

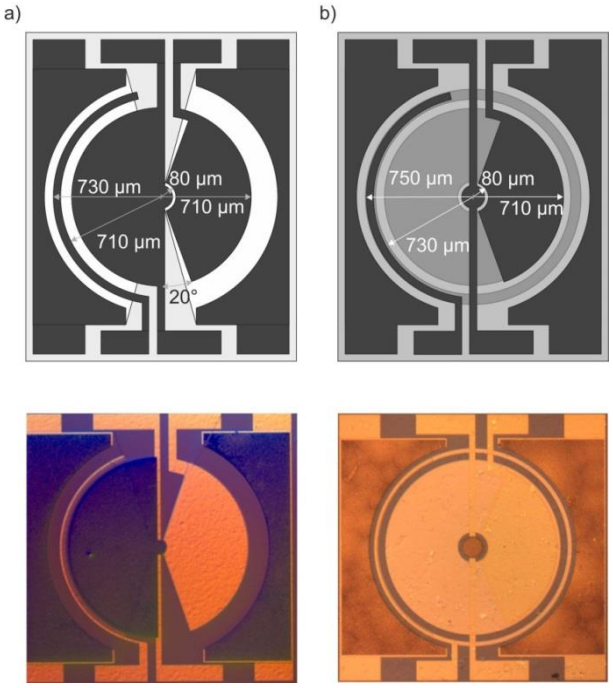


***FIG. 18*** *Top side view of two types of investigated AlGaN/GaN pressure sensors: the sequential ring gate MESA type of sensor (a) and the ring gate $Si_xN_y$ insulating type of MEMS sensor (b).*

We used the customized set up scheme similar as that in [5] which is shown in *FIG. 19*. The dynamic air pressure was applied to the bottom side of the diaphragms. The peak-to-peak pressure amplitude up to 36 kPa was excited at various frequencies (15-1000 Hz) to investigate the frequency dependence of the piezoelectric charge generated on electrodes of the thin AlGaN piezoelectric film. The customized electronic circuit using calibrated pressure gauge measured the amplitude of dynamic air pressure. The laser Doppler vibrometer head *Polytec OFV-302* scanned the velocity of the moving diaphragm.

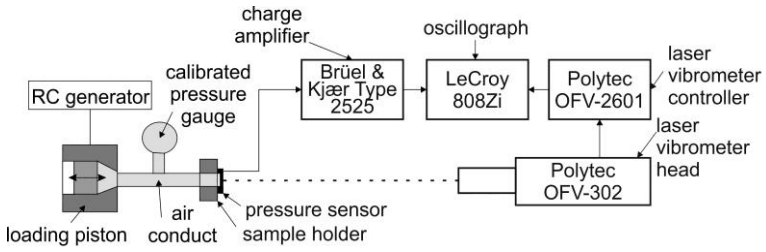


***FIG. 19*** *The experimental set-up scheme used to measure the piezoelectric response of investigated AlGaN/GaN MEMS pressure sensors.*

The output signal from LDV head was processed by the signal controller *Polytec OFV-2601*. The piezoelectric signal generated on the Schottky gate electrodes of the C-HEMT has been read through the signal conditioning circuit of the charge amplifier *Brüel & Kjær Type 2525*. All the output signals were processed and displayed with the digital oscilloscope *LeCroy 808Zi* (*FIG. 20, a)*. Result shows the typical forced vibration of the diaphragm-based pressure sensor excited by the 1.6 kPa peak-to-peak pressure of 45 Hz frequency. The charge is measured on the wide electrode of the $Si_xN_y$ design with the inner and outer radii 80 and 710 µm, respectively. Measured result demonstrates the sensing principle of the piezoelectric MEMS pressure sensor proposed in thesis.

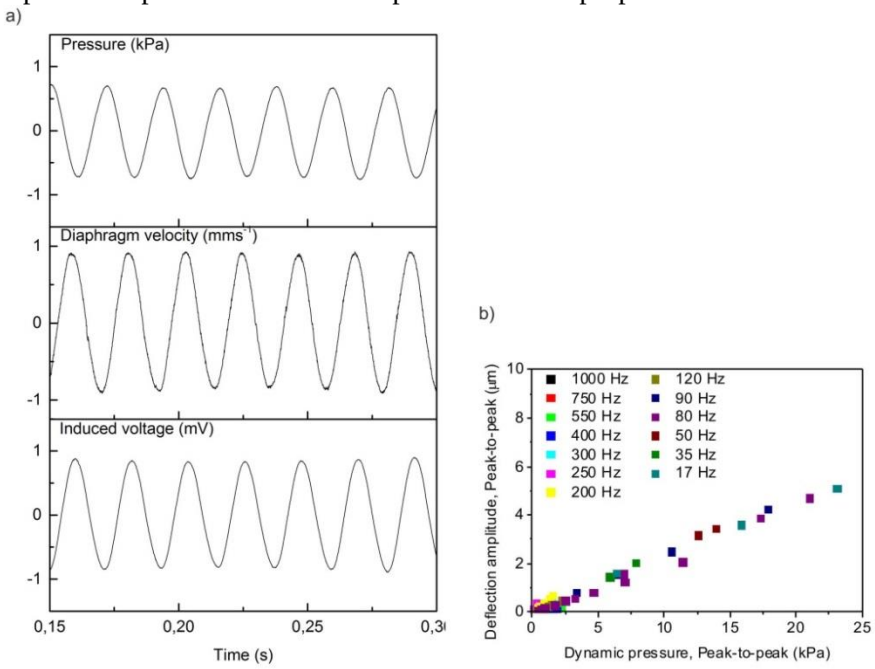


***FIG. 20*** *Typical time response of velocity of the diaphragm center deflection and induced output voltage sensed on wide electrode during the dynamic harmonic pressure loading of the piezoelectric MEMS pressure sensor diaphragm (a) and typical dynamic deflection pressure characteristic of the investigated piezoelectric MEMS pressure sensor (b).*

The phase shift between the diaphragm velocity of deflection and acting pressure (or induced voltage) can be seen what results from forced vibration of the spring mass system. The central deflection of diaphragm can be calculated from the measured velocity as follows:

$$w = \frac{v}{2\pi f}, \tag{3}$$

where $v$ is the measured velocity of diaphragm and $f$ is the frequency of exciting pressure. Typical calculated deflection pressure characteristic of the investigated MEMS sensors is shown in *FIG. 20, b*.

The amplitude of piezoelectric induced charge was calculated from the output voltage of charge amplifier which is proportional to the total input charge:

$$Q = C.V, \tag{4}$$

where $C$ is the reference capacitor (1 nF in selected charge amplifier) and $V$ is the output voltage of amplifier (charge-to-voltage converter), respectively. As a result, the calculated piezoelectric charge of 1 pC corresponds to the 1 mV of the output voltage measured on the ring gate electrode of the sensor. Subsequently, the dependency of induced charge on the frequency of both types of MEMS sensor (*FIG. 18*) was investigated. The frequency of exciting pressure varied in range 15-1000 Hz and the piezoelectric response was measured on wider/inner electrodes located near the source electrodes. In case of MESA sensor (*FIG. 21, a*), the piezoelectric charge is almost frequency independent but some deviations are caused by the electro-mechanical issues of inductive piston which excites the loading pressure. In case of the $Si_xN_y$ sensor, the piezoelectric charge is actually independent from the frequency of exciting load and the sensitivity is considerably improved (*FIG. 21, b*).

Similar results were obtained in our previous works [5, 13] in which the increased gate area of the cantilever based C-HEMT strain sensor caused the improved sensitivity and the measured signal was frequently independent.

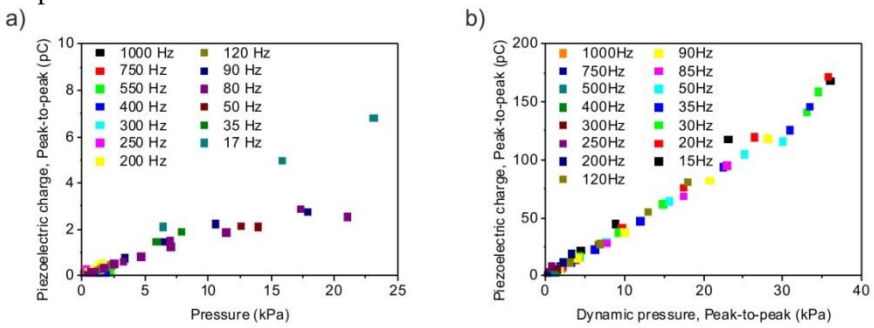


***FIG. 21*** *The piezoelectric induced charge as a response to the external dynamic mechanical load of the MESA (a) and $Si_xN_y$ (b) MEMS pressure sensors at various frequency of load.*

Further, the induced piezoelectric charge was investigated on both sensing electrodes of the $Si_xN_y$ and MESA sensor (*FIG. 22*). The piezoelectric response increased almost linearly with increasing pressure. When comparing the induced charge measured on both electrodes of the $Si_xN_y$ design (*FIG. 22, a*), the higher sensitivity of the wide electrode located closer to the center of diaphragm is observed. Logically, the higher response of induced piezoelectric charge was expected due to the larger scanning area of the wide electrode (1.564 $mm^2$) in compare with the narrow electrode (0.093 $mm^2$) located at the rim of the diaphragm. Finally, the sensitivity of 0.8 pC/kPa and 4.4 pC/kPa was measured for the narrow and wide electrode of this design, respectively.

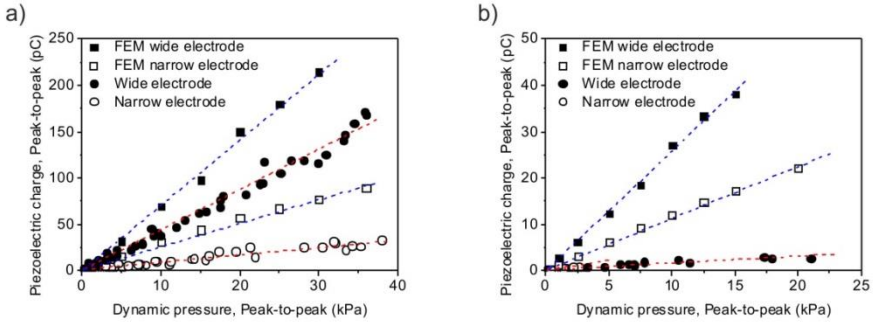


***FIG. 22*** *Measured and simulated piezoelectric charge generated on two different ring gate areas of the C-HEMT: the $Si_xN_y$ design (a) and the MESA design (b).*

When comparing the induced charge measured on both electrodes of the MESA design (*FIG. 22, b*), the higher amount of generated charge is observed on the narrow electrode located at the rim of diaphragm. It is a strange phenomenon whereas this narrow electrode has considerably smaller area (0.035 $mm^2$) in compare with the wide electrode (0.612 $mm^2$) of the MESA sensor. Finally, the sensitivity of 0.34 pC/kPa and 0.16 pC/kPa was determined for the narrow and wide electrode of this design, respectively. We assume that this peculiar behavior may arise from the complex processing technology which may lead in discerption of the thin AlGaN layer located below the Schottky or ohmic electrodes. Thus discontinuous AlGaN cannot create the collecting electrode with sufficiently large area. Moreover, in the MESA design, the mesa etching processing step may lead to decreased 2DEG density [31] due to the partially relaxed AlGaN. We assumed that mesa etching only slightly decreased the density and thus the conductivity of the 2DEG which served as one of the sensing electrodes. Nevertheless, we expected the electrode was still enough conductive to collect the induced charge from piezoelectric material (AlGaN) located between the Schottky gate contact and the 2DEG. Hence and additional mechanical and electrical characterization is required in the future work.

The experiments were supported by the FEM simulation (*FIG. 22*). The 2D axisymmetric models from previous analyses (1000 μm radius, thickness 1.9 μm) were modified considering the new 4.2 μm thick AlGaN/GaN diaphragms with 750 μm radius. The positions of the sensing electrodes in these models were modified according to *FIG. 18*. The previously determined residual stress of 43 MPa was set as an input parameter for the prestressed diaphragm in the FEM models. Finally, the piezoelectric

analysis was performed in which the diaphragms were loaded by the pressure prescribed to their bottom side. The FEM analysis simulated the experimental piezoelectric charge measurement to compare the calculated results with the experimental measurement. A good qualitative agreement in the FEM calculated piezo response is indicated.

Higher sensitivity for both FEM models was simulated (*FIG. 22*). In case of the $Si_xN_y$ sensor, the lower sensitivity of 4.4 pC/kPa and 0.8 pC/kPa for wide and narrow electrode were experimentally obtained, respectively, while the sensitivity of 7.4 pC/kPa and 2.4 pC/kPa were calculated in the FEM simulation. For the MESA design, the identical model was used as for the $Si_xN_y$ design. Only the radii of the sensing electrodes changed according to dimensions in *FIG. 18, a*. However, the simulated charge was multiplied by the equivalent area of the sequential electrode. Area of the sequential gate electrode (140 ° angle) compared to that of the full ring electrode (360 °) is smaller and therefore the generated charge was multiplied by the number expressing the ratio of these two angles: 140 °/360 °= 0.389. A substantial deviation in the FEM calculated piezoresponse is indicated in *FIG. 22, b* when compared with results of the experimental measurement. In the FEM analysis, the sensitivity of 2.9 pC/kPa and 0.94 pC/kPa were calculated for wide and narrow electrode of the MESA type of sensor, respectively. But in the experimental measurement, only sensitivity 0.16 pC/kPa and 0.34 pC/kPa were obtained for wide and narrow electrode, respectively.

It has been mentioned that the positions of the sensing electrodes for two modeled designs were optimized for the 1.9 µm thick diaphragms which were previously used and not for the diaphragms with increased thickness 4.2 µm. Therefore two electrodes located on the top surface of diaphragms of the $Si_xN_y$ or MESA sensor exhibits different sensitivities. It is possible to prove that the same sensitivity of the inner and outer electrode can be achieved using the proper design of the electrodes (*FIG. 23*).

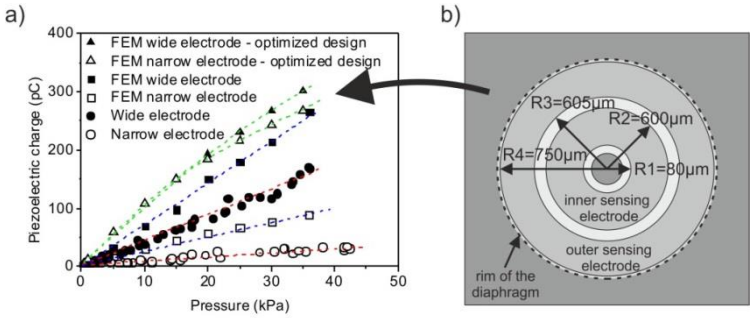


***FIG. 23*** *Simulated and measured piezoresponse induced in two different ring gate areas of the sensor. Triangles (a) represent the charge simulated on the electrodes of the optimal $Si_xN_y$ design (b).*

If the results depicted in *FIG. 17, b* were taken into account, the ideal inner and outer radius of the inner/wide sensing electrode would be 80 µm and 600 µm, respectively. Then the outer electrode could have the inner and outer radii 605 µm and 750 µm for instance. These would be the optimized electrode dimensions for the 4.2 µm thick AlGaN/GaN diaphragm based on the results of FEM analysis in which the distribution of the mechanical stresses was investigated. Another FEM simulation can be performed using of this modified radii of the sensing electrodes. The resulted piezoelectric charge collected on the inner Schottky electrode would have nearly the same amplitude as that collected from the outer Schottky sensing electrode (*FIG. 23, a*). Now, these two curves show the highest possible generated charge from the MEMS pressure sensor. Therefore the design with the sensing electrodes with dimensions according to *FIG. 23, b* can be labeled as the most effective design of the AlGaN/GaN piezoelectric MEMS pressure sensor.

### *4.3.3. Critical pressure*

In addition, the maximum pressure load, i.e. critical pressure of the MEMS pressure sensor was investigated. It means the pressure that can be applied to the sensor without causing the diaphragms catastrophic failure. The experimental set-up scheme as used previously (*FIG. 19*) was complemented by the video camera. The diaphragm was loaded to its bottom side while the pressure gauge measured the actual pressure of air. The pressure in the system was dynamically changed by compressing the hand air pump. Signal from pressure gauge was displayed and recorded on the oscilloscope (*FIG. 24*).

A moment when the diaphragm ruptured was recorded. The critical pressure with peak amplitude 21.5 kPa was measured. The experiment was supported by the FEM analysis. The structural analysis was performed using of the previously created model. The diaphragm was loaded by the static pressure to its bottom side.

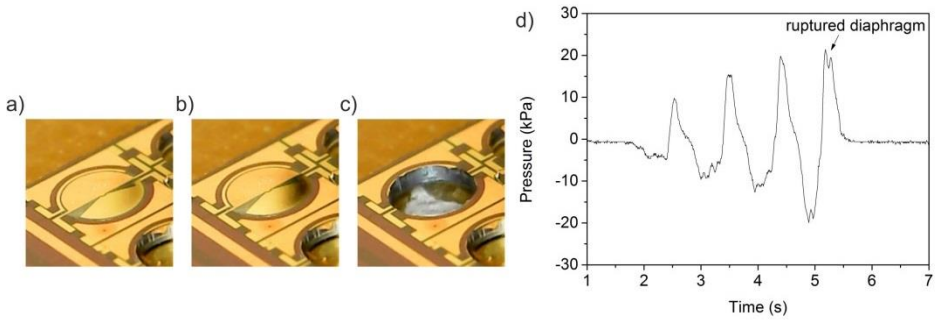


***FIG. 24*** *Test of maximum (critical) pressure for the proposed MEMS pressure sensor in which the pressure increased (a-b) until the diaphragm ruptured (c). Critical pressure 21.5 kPa was read from resulted graph (d).*

The amplitude of pressure was increased until the stress generated in the diaphragm achieved the maximal strength of GaN [22]. The FEM analysis revealed the maximum peak amplitude 30 kPa. The result of FEM simulation showed to be 40 % higher than experimentally measured value 21.5 kPa. We assumed that the deviation is due to the idealized model used in the FEM analysis. The diaphragm of the real device may contain microstructural defects which cannot be seen by naked eye or by common optical microscope and are neglected in the FEM model.

## Summary

The pressure sensor presented in this thesis has been developed in Department of Microelectronic Structures at Institute of Electrical Engineering of Slovak Academy of Sciences. It has been solved within the Slovak Research and Development Agency project under contract APVV-0450-10.

Compared to the other commonly used piezoelectrics, the AlGaN/GaN heterostructure enables the operation in harsh environment while the integration with standard integrated circuits (IC) technology is maintained. In this thesis we investigated the novel method to sense the differential pressure using of the AlGaN/GaN diaphragms. The conductive two dimensional electron gas (2DEG) channel created in AlGaN/GaN heterostructure was used as a first collector of induced piezoelectric charge. The second top collecting electrode was created by the ring gate electrode of the C-HEMT sensing device. Such new construction design of the sensing device has become unique and innovative approach in pressure sensing adopting of the AlGaN/GaN heterostructure as a thin piezoelectric layer. A bulk micromachining of the supporting Si substrate by DRIE was used to create the diaphragm-based structure. Two different design constructions of diaphragm-based MEMS pressure sensor were developed. The first one is based on the mesa isolation and is called the MESA sensor with sequential ring gate electrodes. The second one, based on the $Si_xN_y$ insulating/passivation layer, is called the $Si_xN_y$ sensor with ring gate electrodes. The designs of the diaphragm based AlGaN/GaN pressure sensors were based on the results of finite element method (FEM) analyses. Moreover, the FEM analyses along with two experimental methods (resonant method and bulging technique) were successfully performed to determine the residual stress in diaphragms of the MEMS pressure sensor. It has been shown that all the investigated diaphragms were tensile stretched. Calculated residual stress was then used in following piezoelectric FEM simulations.

The main goal of this thesis was to verify the functionality of proposed piezoelectric MEMS pressure sensor. The different designs of the diaphragm-based pressure sensors with 1500 μm diameter were experimentally examined. In case of the $Si_xN_y$ design, a good qualitative agreement of the FEM calculated piezo response with the experiment was observed. Nevertheless the higher sensitivity of the FEM model was calculated when compared to experiments. A considerable higher sensitivity of the FEM model compared to that of experiment was obtained in case of the MESA design. In the FEM analysis, the result showed the higher sensitivity of the inner/wide electrode whereas the experimental measurement showed the opposite result.

Based on the result mentioned above, it is recommended to work with the optimal $Si_xN_y$ design in the future. Further experiments should be devoted to test operation of the MEMS pressure sensors in harsh environment. Especially the operation at high temperatures and long-time reliability should be verified. The proposed AlGaN/GaN piezoelectric MEMS pressure sensor may be then prepared for integration with additional electronic circuits into a single chip. In the future, the proposed MEMS pressure sensor can be relatively simply modified and potentially used in many applications for pressure sensing in harsh environment, e.g. in the wings of an aircraft, in combustion engine, exhaust, etc.

The originality and innovative research of the AlGaN/GaN piezoelectric MEMS pressure sensor described in thesis was validated by the international patent application: WO2015049598 (A1) - MEMS Pressure sensor with a high electron mobility transistor and a production method thereof.

# Súhrn

Mikro-elektro-mechanický (MEMS) tlakový senzor prezentovaný v dizertačnej práci bol vyvíjaný na Oddelení mikroelektronických štruktúr na Elektrotechnickom ústave Slovenskej akadémie vied. Problematika tlakového senzora pre agresívne prostredia bola riešená v rámci projektu podporovaného Agentúrou na podporu výskumu a vývoja na základe zmluvy č. APVV-450-10. Heteroštruktúra AlGaN/GaN sa postupne stáva čoraz populárnejšou v aplikáciách v senzorike vďaka jej výnimočným vlastnostiam. V porovnaní s bežne používanými piezoelektrickými materiálmi je funkčná v agresívnych prostrediach, t.j. pri zvýšených teplotách a v chemicky agresívnom prostredí, zatiaľ čo je zachovaná možnosť integrácie s elektronickými obvodmi.

Dizertačná práca sa zaoberá originálnou metódou snímania tlaku s použitím membránového snímača tvoreného AlGaN/GaN materiálovým systémom. Dvojrozmerný vodivý elektrónový plyn (2DEG), tvoriaci kanál tranzistora, bol použitý ako jedna zberná elektróda pre generovaný piezoelektrický náboj. Druhá elektróda je tvorená hradlovou elektródou C-HEMT prvku. Membránová štruktúra bola vytvorená objemovým obrábaním kremíkového substrátu metódou hlbokého iónového leptania (DRIE). Vytvorené boli dva rôzne typy tlakového senzora. Prvým typom je MESA tlakový senzor na báze „mesa“ izolačného leptania tenkých vrstiev, pre ktorý je charakteristický tvar sekvenčných prstencových snímacích elektród. Druhým navrhnutým typom je $Si_xN_y$ membránový tlakový senzor, založený na pasivačnej/izolačnej vrstve $Si_xN_y$ a jeho charakteristickým prvkom sú prstencové elektródy s väčšou snímacou plochou v porovnaní s MESA typom senzora.

Dizajn AlGaN/GaN membránového tlakového senzora bol navrhovaný na základe výsledkov z analýzy metódou konečných prvkov (MKP). Spolu s dvoma experimentálnymi metódami (rezonančná a deflekčná metóda) bola MKP analýza použitá na určenie reziduálneho napätia v membránach MEMS tlakového senzora. Ukázalo sa, že všetky membrány sú napnuté pomerne nízkym ťahovým napätím. Na základe experimentálne zistených hodnôt reziduálneho napätia boli vytvorené MKP modely senzora.

Hlavným cieľom dizertačnej práce bola verifikácia funkčnosti rôznych typov navrhovaného MEMS tlakového senzora. Aj napriek vyššej simulovanej piezoelektrickej odozve bola dosiahnutá dobrá kvalitatívna zhoda s výsledkami experimentov, a to najmä v prípade $Si_xN_y$ typu senzora. V prípade MESA typu senzora bola simulovaná výrazne vyššia piezoelektrická odozva oproti nameranej odozve.

Na základe poznatkov získaných pri riešení problematiky prezentovaného MEMS tlakového senzora sa v budúcnosti odporúča využitie optimálneho dizajnu $Si_xN_y$ senzora. Nasledujúce experimenty môžu byť zamerané na funkčnosť senzora umiestneného do agresívneho prostredia. Predovšetkým by mala byť overená schopnosť MEMS senzora pracovať pri zvýšenej teplote okolitého prostredia a jeho dlhodobá spoľahlivosť. Navrhnutý AlGaN/GaN piezoelektrický MEMS tlakový senzor môže byť následne pripravený na integráciu s aditívnym elektronickým obvodom do jedného spoločného čipu a potenciálne využitý pre snímanie tlaku v agresívnych prostrediach, napr. v leteckom priemysle, spaľovacích motoroch, výfukoch atď.

Originalita a inovatívny výskum AlGaN/GaN piezoelektrického MEMS tlakového senzora prezentovaného v dizertačnej práci sú potvrdené medzinárodnou patentovou prihláškou: WO2015049598 (A1) - MEMS Pressure sensor with a high electron mobility transistor and a production method thereof.

# References


1. PEARTON, S. J, ABERNATHY, C. R and REN, Fan. *Gallium nitride processing for electronics, sensors and spintronics*. London : Springer, 2006. ISBN 9781846283598 1846283590 1852339357 9781852339357.
2. PEARTON, S J, KANG, B S, KIM, Suku, REN, F, GILA, B P, ABERNATHY, C R, LIN, Jenshan and CHU, S N G. GaN-based diodes and transistors for chemical, gas, biological and pressure sensing. *Journal of Physics: Condensed Matter*. 28 July 2004. Vol. 16, no. 29, p. R961–R994. DOI 10.1088/0953-8984/16/29/R02.
3. CIMALLA, V, PEZOLDT, J and AMBACHER, O. Group III nitride and SiC based MEMS and NEMS: materials properties, technology and applications. *Journal of Physics D: Applied Physics*. 21 October 2007. Vol. 40, no. 20, p. 6386–6434. DOI 10.1088/0022-3727/40/20/S19.
4. VANKO, Gabriel, DRŽÍK, Milan, VALLO, Martin, LALINSKÝ, Tibor, KUTIŠ, Vladimír, STANČÍK, Stanislav, RÝGER, Ivan and KOSTIČ, Ivan. AlGaN/GaN C-HEMT structures for dynamic stress detection. *Procedia Engineering*. 2010. Vol. 5, p. 1405–1408. DOI 10.1016/j.proeng.2010.09.378.
5. LALINSKÝ, T., DRŽÍK, M., VANKO, G., VALLO, M., KUTIŠ, V., BRUNCKO, J., HAŠČÍK, š., JAKOVENKO, J. and HUSÁK, M. Piezoelectric response of AlGaN/GaN-based circular-HEMT structures. *Microelectronic Engineering*. August 2011. Vol. 88, no. 8, p. 2424–2426. DOI 10.1016/j.mee.2010.12.013.
6. LIU, Y., KAUSER, M. Z., NATHAN, M. I., RUDEN, P. P., DOGAN, S., MORKOÇ, H., PARK, S. S. and LEE, K. Y. Effects of hydrostatic and uniaxial stress on the Schottky barrier heights of Ga-polarity and N-polarity n-GaN. *Applied Physics Letters*. 2004. Vol. 84, no. 12, p. 2112. DOI 10.1063/1.1689392.
7. LIU, Y., KAUSER, M. Z., RUDEN, P. P., HASSAN, Z., LEE, Y. C., NG, S. S. and YAM, F. K. Effect of hydrostatic pressure on the barrier height of Ni Schottky contacts on n-AlGaN. *Applied Physics Letters*. 2006. Vol. 88, no. 2, p. 022109. DOI 10.1063/1.2164909.
8. LIU, Y., KAUSER, M. Z., SCHROEPFER, D. D., RUDEN, P. P., XIE, J., MOON, Y. T., ONOJIMA, N., MORKOÇ, H., SON, K.-A. and NATHAN, M. I. Effect of hydrostatic pressure on the current-voltage characteristics of GaN⁄AlGaN⁄GaN heterostructure devices. *Journal of Applied Physics*. 2006. Vol. 99, no. 11, p. 113706. DOI 10.1063/1.2200742.
9. LIU, Y., RUDEN, P. P., XIE, J., MORKOÇ, H. and SON, K.-A. Effect of hydrostatic pressure on the dc characteristics of AlGaN⁄GaN heterojunction field effect transistors. *Applied Physics Letters*. 2006. Vol. 88, no. 1, p. 013505. DOI 10.1063/1.2161812.
10. EICKHOFF, M., AMBACHER, O., KRÖTZ, G. and STUTZMANN, M. Piezoresistivity of Al[sub x]Ga[sub 1−x]N layers and Al[sub x]Ga[sub 1−x]N/GaN heterostructures. *Journal of Applied Physics*. 2001. Vol. 90, no. 7, p. 3383. DOI 10.1063/1.1398602.
11. KANG, B. S., KIM, S., KIM, J., REN, F., BAIK, K., PEARTON, S. J., GILA, B. P., ABERNATHY, C. R., PAN, C.-C., CHEN, G.-T., CHYI, J.-I., CHANDRASEKARAN, V., SHEPLAK, M., NISHIDA, T. and CHU, S. N. G. Effect of external strain on the conductivity of AlGaN/GaN high-electron-mobility transistors. *Applied Physics Letters*. 2003. Vol. 83, no. 23, p. 4845. DOI 10.1063/1.1631054.
12. CHIA-TA CHANG, SHIH-KUANG HSIAO, CHANG, E.Y., CHUNG-YU LU, JUI-CHIEN HUANG and CHING-TING LEE. Changes of Electrical Characteristics for AlGaN/GaN HEMTs Under Uniaxial Tensile Strain. *IEEE Electron Device Letters*. March 2009. Vol. 30, no. 3, p. 213–215. DOI 10.1109/LED.2009.2012447.
13. VANKO, Gabriel, DRŽÍK, Milan, VALLO, Martin, LALINSKÝ, Tibor, KUTIŠ, Vladimír, STANČÍK, Stanislav, RÝGER, Ivan and BENČUROVÁ, Anna. AlGaN/GaN C-HEMT structures for dynamic stress detection. *Sensors and Actuators A: Physical*. December 2011. Vol. 172, no. 1, p. 98–102. DOI 10.1016/j.sna.2011.02.049.
14. LALINSKÝ, T., VANKO, G., VALLO, M., DRŽÍK, M., BRUNCKO, J., JAKOVENKO, J., KUTIŠ, V., RÝGER, I., HAŠČÍK, š. and HUSÁK, M. Impact of ZnO gate interfacial layer on piezoelectric response of AlGaN/GaN C-HEMT based ring gate capacitor. *Sensors and Actuators A: Physical*. December 2011. Vol. 172, no. 2, p. 386–391. DOI 10.1016/j.sna.2011.09.028.
15. LALINSKÝ, T., VALLO, M., VANKO, G., DOBROČKA, E., VINCZE, A., OSVALD, J., RÝGER, I. and DZUBA, J. Iridium oxides based gate interface of AlGaN/GaN high electron mobility transistors formed by high temperature oxidation. *Applied Surface Science*. October 2013. Vol. 283, p. 160–167. DOI 10.1016/j.apsusc.2013.06.069.
16. LE BOULBAR, E.D., EDWARDS, M.J., VITTOZ, S., VANKO, G., BRINKFELDT, K., RUFER, L., JOHANDER, P., LALINSKÝ, T., BOWEN, C.R. and ALLSOPP, D.W.E. Effect of bias conditions on pressure sensors based on AlGaN/GaN High Electron Mobility Transistor. *Sensors and Actuators A: Physical*. May 2013. Vol. 194, p. 247–251. DOI 10.1016/j.sna.2013.02.017.
17. ZIMMERMANN, T., NEUBURGER, M., BENKART, P., HERNANDEZ-GUILLEN, F.J., PIETZKA, C., KUNZE, M., DAUMILLER, I., DADGAR, A., KROST, A. and KOHN, E. Piezoelectric GaN sensor structures. *IEEE Electron Device Letters*. May 2006. Vol. 27, no. 5, p. 309–312. DOI 10.1109/LED.2006.872918.
18. KANG, B. S., KIM, S., REN, F., JOHNSON, J. W., THERRIEN, R. J., RAJAGOPAL, P., ROBERTS, J. C., PINER, E. L., LINTHICUM, K. J., CHU, S. N.G., BAIK, K., GILA, B. P., ABERNATHY, C. R. and PEARTON, S. J. Pressure-induced changes in the conductivity of AlGaN⁄GaN high-electron mobility-transistor membranes. *Applied Physics Letters*. 2004. Vol. 85, no. 14, p. 2962. DOI 10.1063/1.1800282.
19. KANG, B. S., KIM, J., JANG, S., REN, F., JOHNSON, J. W., THERRIEN, R. J., RAJAGOPAL, P., ROBERTS, J. C., PINER, E. L., LINTHICUM, K. J., CHU, S. N. G., BAIK, K., GILA, B. P., ABERNATHY, C. R. and PEARTON, S. J. Capacitance pressure sensor based on GaN high-electron-mobility transistor-on-Si membrane. *Applied Physics Letters*. 2005. Vol. 86, no. 25, p. 253502. DOI 10.1063/1.1952568.
20. STRITTMATTER, R. P., BEACH, R. A., BROOKE, J., PREISLER, E. J., PICUS, G. S. and MCGILL, T. C. GaN Schottky diodes for piezoelectric strain sensing. *Journal of Applied Physics*. 2003. Vol. 93, no. 9, p. 5675. DOI 10.1063/1.1558960.
21. LALINSKÝ, T., HUDEK, P., VANKO, G., DZUBA, J., KUTIŠ, V., SRNÁNEK, R., CHOLEVA, P., VALLO, M., DRŽÍK, M., MATAY, L. and KOSTIČ, I. Micromachined membrane structures for pressure sensors based on AlGaN/GaN circular HEMT sensing device. *Microelectronic Engineering*. October 2012. Vol. 98, p. 578–581. DOI 10.1016/j.mee.2012.06.014.
22. PANKOVE, Jacques I. (ed.). *Gallium nitride (GaN). 2: [...]*. San Diego, Calif. : Acad. Press, 1999. Semiconductors and semimetals, 57. ISBN 9780127521664 0127521666 012544057X.
23. DZUBA, J, VANKO, G, DRŽÍK, M, RÝGER, I, VALLO, M, KUTIŠ, V, HAŠKO, D, CHOLEVA, P and LALINSKÝ, T. Stress investigation of the AlGaN/GaN micromachined circular diaphragms of a pressure sensor. *Journal of Micromechanics and Microengineering*. 1 January 2015. Vol. 25, no. 1, p. 015001. DOI 10.1088/0960-1317/25/1/015001.
24. SHEPLOAK, M. and DUGUNDJI, J. Large Deflections of Clamped Circular Plates Under Initial Tension and Transitions to Membrane Behavior. *Journal of Applied Mechanics*. 1998. Vol. 65, no. 1, p. 107. DOI 10.1115/1.2789012.
25. YU, M. and BALACHANDRAN, B. Sensor diaphragm under initial tension: Linear analysis. *Experimental Mechanics*. April 2005. Vol. 45, no. 2, p. 123–129. DOI 10.1007/BF02428184.
26. MALHAIRE, C. Comparison of two experimental methods for the mechanical characterization of thin or thick films from the study of micromachined circular diaphragms. *Review of Scientific Instruments*. 2012. Vol. 83, no. 5, p. 055008. DOI 10.1063/1.4719964.

27. YANG, Z., WANG, R. N., JIA, S., WANG, D., ZHANG, B. S., LAU, K. M. and CHEN, K. J. Mechanical characterization of suspended GaN microstructures fabricated by GaN-on-patterned-silicon technique. *Applied Physics Letters*. 2006. Vol. 88, no. 4, p. 041913. DOI 10.1063/1.2167813.
28. PAN, Xiaojun, TAN, Chee Wee, MIAO, Jianmin, KASIM, Johnson, SHEN, Zexiang and XIE, Erqing. The stress analysis of Si MEMS devices by micro-Raman technique. *Thin Solid Films*. July 2009. Vol. 517, no. 17, p. 4905–4908. DOI 10.1016/j.tsf.2009.03.120.
29. VLASSAK, J. J. and ENGINEERING, Stanford University Dept of Materials Science and. *New Experimental Techniques and Analysis Methods for the Study of the Mechanical Properties of Materials in Small Volumes* [online]. Stanford University, 1994. Available from: https://books.google.sk/books?id=Hh7-PQAACAAJ
30. AMBACHER, O, MAJEWSKI, J, MISKYS, C, LINK, A, HERMANN, M, EICKHOFF, M, STUTZMANN, M, BERNARDINI, F, FIORENTINI, V, TILAK, V, SCHAFF, B and EASTMAN, L F. Pyroelectric properties of Al(In)GaN/GaN hetero- and quantum well structures. *Journal of Physics: Condensed Matter*. 8 April 2002. Vol. 14, no. 13, p. 3399–3434. DOI 10.1088/0953-8984/14/13/302.
31. CHU, S.N.G., REN, F., PEARTON, S.J., KANG, B.S., KIM, S., GILA, B.P., ABERNATHY, C.R., CHYI, J.-I., JOHNSON, W.J. and LIN, J. Piezoelectric polarization-induced two dimensional electron gases in AlGaN/GaN heteroepitaxial structures: Application for micro-pressure sensors. *Materials Science and Engineering: A*. November 2005. Vol. 409, no. 1-2, p. 340–347. DOI 10.1016/j.msea.2005.05.119.

# Author's publications

### 2015

- **Dzuba, J.**, Vanko, G., Držík, M., Rýger, I., Vallo, M., Kutiš, V., Haško, D., Choleva, P., Lalinský, T., : Stress investigation of the AlGaN/GaN micromachined circular diaphragms of a pressure sensor. J. Micromech. Microengn. 25 (2015) 015001.

### 2014

- Vanko, G., Vojs, M., Ižák, T., Potocký, P., Choleva, P., Marton, M., Rýger, I., **Dzuba, J.**, Lalinský, T., : AlGaN/GaN micromembranes with diamond coating for high electron mobility transistors operated at high temperatures In: ASDAM 2014. Eds. J. Breza et al. IEEE 2014. ISBN 978-1-4799-5474-2. P. 263-266.
- Rýger, I., Vanko, G., Lalinský, T., **Dzuba, J.**, Vallo, M., Kunzo, P., Vávra, I., : Enhanced sensitivity of Pt/NiO gate based AlGaN/GaN C-HEMT hydrogen sensor Key Engn. Mater. 605 (2014) 491-494.
- **Dzuba, J.**, Vanko, G., Rýger, I., Vallo, M., Kutiš, V., Lalinský, T., : Influence of temperature on the sensitivity of the AlGaN/GaN C HEMT based piezoelectric pressure sensor In: ASDAM 2014. Eds. J. Breza et al. IEEE 2014. ISBN 978-1-4799-5474-2. P. 5-8.
- **Dzuba, J.**, Držík, M., Vanko, G., Rýger, I., Vallo, M., Kutiš, V., Lalinský, T., : Modal analysis of Gallium Nitride membrane for pressure sensing device Key Engn. Mater. 605 (2014) 404-407.
- Vanko, G., **Dzuba, J.**, Rýger, I., Lalinský, T., Vojs, M., Vincze, A., Dobročka, E., : Processing technology of MEMS sensors using III-N material system In: 17. škola vákuovej techniky: Analýza materiálov vo vákuu. Material analysis in vacuum. Eds. M. Michalka et al. Bratislava: FEI STU 2014. ISBN 978-80-971179-4-8. P. 39-43.
- **Dzuba, J.**, Vanko, G., Držík, M., Rýger, I., Vallo, M., Lalinský, T., Kutiš, V., Haško, D., Srnánek, R., : The AlGaN/GaN C-HEMT diaphragm-based MEMS pressure sensor for harsh environment In: 17. škola vákuovej techniky: Analýza materiálov vo vákuu. Material analysis in vacuum. Eds. M. Michalka et al. Bratislava: FEI STU 2014. ISBN 978-80-971179-4-8. P. 142-145.
- Zehetner, J., Vanko, G., Choleva, P., **Dzuba, J.**, Rýger, I., Lalinský, T., : Using of laser ablation technique in the processing technology of GaN/SiC based MEMS for extreme conditions In: ASDAM 2014. Eds. J. Breza et al. IEEE 2014. ISBN 978-1-4799-5474-2. P. 259-262.

### 2013

- Vanko, G., Lalinský, T., Ižák, T., Vojs, M., Vincze, A., Dobročka, E., Vallo, M., **Dzuba, J.**, Rýger, I., Kromka, A., : AlGaN/GaN high electron mobility transistors for high temperatures In: Perspektívne vákuové metódy a technológie: 16. škola vákuovej techniky. Eds. M. Vojs, M. Veselý. Bratislava: Slov. vákuová spol. 2013. ISBN 978-80-971179-2-4. S. 55-59.
- Vanko, G., Hudek, P., **Dzuba, J.**, Choleva, P., Kutiš, V., Vallo, M., Rýger, I., Lalinský, T., : Bulk micromachining of SiC substrate for MEMS sensor applications. Microelectron. Engn. 110 (2013) 260-264.
- Lalinský, T., Vallo, M., Vanko, G., Dobročka, E., Vincze, A., Osvald, J., Rýger, I., **Dzuba, J.**, : Iridium oxides based gate interface of AlGaN/GaN high electron mobility transistors formed by high temperature oxidation. Applied Surface Sci 283 (2013) 160-167.

- Vanko, G., Hudek, P., Zehetner, J., **Dzuba, J.**, Choleva, P., Vallo, M., Rýger, I., Lalinský, T., : MEMS pressure sensor fabricated by advanced bulk micromachining techniques, Proc. SPIE 8763 (2013) 8763-101.
- Kutiš, V., **Dzuba, J.**, Paulech, J., Murín, J., Hrabovský, J., Lalinský, T., : Piezoelectric analysis of MEMS pressure sensor. In: Proc. 19th Inter. Conf. on Applied Phys. of Cond. Matter (APCOM 2013). Eds. J. Vajda and I. Jamnický. Bratislava: FEI STU 2013. ISBN 978-80-227-3956-6. P. 225-228.

### 2012

- Vanko, G., Vallo, M., Rýger, I., **Dzuba, J.**, Lalinský, T., : Conductive metal oxide based gates for self-aligned technology of AlGaN/GaN HEMT. In: ASDAM 2012. Eds. Š. Haščík, J. Osvald. Piscataway: IEEE 2012. ISBN 978-1-4673-1195-3. P. 19-22.
- Rýger, I., Vanko, G., Kunzo, P., Lalinský, T., **Dzuba, J.**, Vallo, M., Satrapinsky, L., Plecenik, T., Chvála, A., : Gates of AlGaN/GaN HEMT for high temperature gas sensing applications. In: ASDAM 2012. Eds. Š. Haščík, J. Osvald. Piscataway: IEEE 2012. ISBN 978-1-4673-1195-3. P. 23-26.
- Kutiš, V., **Dzuba, J.**, Paulech, J., Murín, J., Lalinský, T., : MEMS piezoelectric pressure sensor-modelling and simulation. Procedia Engn. 48 (2012) 338-345.
- Lalinský, T., Hudek, P., Vanko, G., **Dzuba, J.**, Kutiš, V., Srnánek, R., Choleva, P., Vallo, M., Držík, M., Matay, L., Kostič, I., : Micromachined membrane structures for pressure sensors based on AlGaN/GaN circular HEMT sensing device. Microelectron. Engn. 98 (2012) 578–581.
- **Dzuba, J.**, Lalinský, T., Vanko, G., Vallo, M., Rýger, I., Kutiš, V., Královič, V., : Modeling and simulation of AlGaN/GaN piezoelectric MEMS pressure sensor. In: 13th Mechatronics Forum Inter. Conf. – Mechatronics 2012. Linz 2012. P. 773-778.

## Citations

- Vanko, G., Hudek, P., **Dzuba, J.**, Choleva, P., Kutiš, V., Vallo, M., Rýger, I., Lalinský, T., : Bulk micromachining of SiC substrate for MEMS sensor applications. Microelectron. Engn. 110 (2013) 260-264. (SK-AT-0019-10). (APVV 0450-10). (APVV 0199-10). (VEGA-2-0163-09).
    1. *Olhero, S. M.: Mater. Research Bull. 60 (2014) 830.*
    2. *Preusch, F.: Micromachines 5 (2014) 1051.*
    3. *Leclaire, P.: Semicond. Sci Technol. 29 (2014) 115018.*
    4. *Frischmuth, T.: Procedia Engn. 87 (2014) 128.*

- Kutiš, V., **Dzuba, J.**, Paulech, J., Murín, J., Lalinský, T., : MEMS piezoelectric pressure sensor-modelling and simulation. Procedia Engn. 48 (2012) 338-345. (APVV 0450-10).
    1. *Ganji, M.: Inter. J. Modell. Simul. 33 (2013) 15.*

- Lalinský, T., Hudek, P., Vanko, G., **Dzuba, J.**, Kutiš, V., Srnánek, R., Choleva, P., Vallo, M., Držík, M., Matay, L., Kostič, I., : Micromachined membrane structures for pressure sensors based on AlGaN/GaN circular HEMT sensing device. Microelectron. Engn. 98 (2012) 578–581. (APVV 0655-07). (APVV 0450-10). (APVV 0199-10). (VEGA-2-0163-09).
    1. *Ko, S.C.: J. Micromech. Microengn. 23 (2013) 035011.*
    2. *Wang, C.: Microelectr. Engn. 109 (2013) 24.*
    3. *Linganiso, E.C.: Mater. Chem. Phys. 143 (2013) 367.*
    4. *Haehnlein, B.: Phys. Status Solidi C 11 (2014) 239.*
    5. *Al-Shibaany, Z.Y.A.: IOP Conf. Ser. 65 (2014) 012030.*
    6. *Tiginyanu, I.: Turkish J. Phys. 38 (2014) 328.*